

BioRID-II Dummy Model Development

--

Stochastic Investigations

Sebastian Stahlschmidt*, Bastian Keding*, K. Witowski*, H. Müllerschön*, U. Franz*

*DYNAmore GmbH, Stuttgart, Germany

Abstract:

Whiplash injuries frequently occur in low speed rear crashes. Many consumer and insurance organizations use the BioRID-II dummy as test device, to assess the risk of whiplash injuries in car accidents. An LS-DYNA model of the BioRID-II dummy has been developed by DYNAmore GmbH in cooperation with the German Automotive Industry.

This paper describes the current validation state and describes the latest modifications of the BioRID-II model. The emphasis is to discuss observations made during validation. Finally, the paper describes a robustness study of one selected validation load case. The investigation was performed to learn about dependencies and stability of the measured quantities.

Keywords:

BioRID, Dummy, whiplash, robustness, oscillation, neck link rotation

1 Introduction

Whiplash [1] is an injury that often occurs in low speed rear impact scenarios in passenger cars. Already in the 80th the interest for whiplash investigations was increasing significantly. At this time only the H3-50 Dummy with his very stiff thorathic spine and its simple neck was available for whiplash investigations. This Dummy was limited to capture injury criteria for whiplash scenarios.

In the 1090's the Chalmers University of Technology of Sweden developed in corporation with Saab and Volvo the BioRID. The dummy is equipped with a detailed flexible spine and neck to predict injury risks in rear impacts. Since it allows estimating the whiplash risk the dummy is used in insurance and consumer tests to assess seat designs. The majority of the considered tests use the BioRID-II dummy, which is an enhanced version of the BioRID, in a low speed rear sled tests in a sled test with a pre-defined pulse.

Due to the dominantly elastic deformations in the seat during the whiplash tests, it is very difficult to detect the different load paths between the Dummy and the seat. In tests with high plastic deformation modes important information can be gained after the test. Unfortunately, this is not possible for the tests with the BioRID-II dummy. Hence, by simulations important knowledge could be gained to understand the interaction of the parts. Therefore, a working group of the FAT (German Association for Automotive Research) has been launched in 2004 to develop a finite element model of the BioRID-II. Participating companies are Audi, BMW, Mercedes, Porsche, Keiper Recaro, Hammerstein, Johnson Controls, Volkswagen and Karmann. During the project the FAT is defining tests, requirements and approves the model based on the milestones. Like in former dummy modeling projects DYNAmore is responsible for developing the LS-DYNA model. The model is commercially available for companies not participating the working group.

Previous releases of the model and the project itself has been presented in papers already. The aim of this paper is to describe current work performed during the validation. The emphasis of the presented graphs is to showcase effects rather than presenting the performance in the various tests. The correlation in the entire set of component and sled tests is presented in [2]. Beside the description of used new features the paper presents a stochastic investigation performed to understand the dummy behavior and stability.

2 Model outline and latest modifications

The current commercial release of the BioRID II model is version 1.5. It is available since May 2006. The model is based on CAD data from the dummy manufacturer Denton CAE for the BioRID-II specific parts and scanned data for parts also used in Hybrid III dummies. The masses are adapted according to a detailed measurement of each part.

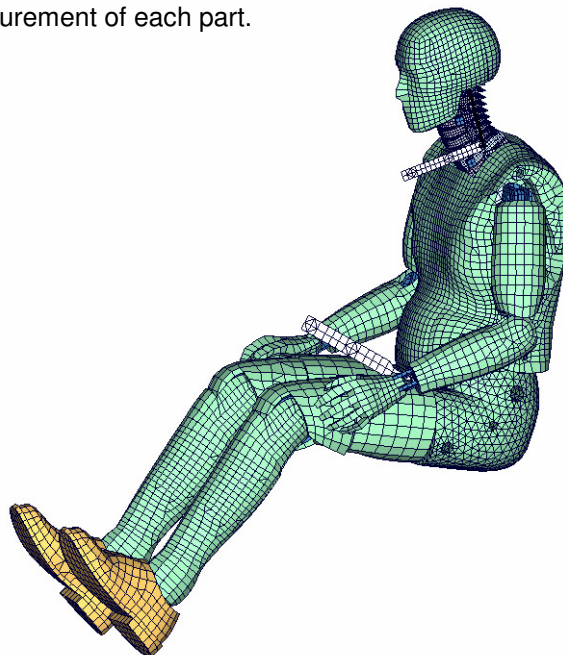


Figure 1: FAT LS-DYNA BioRID II dummy model release 1.5.

Release 1.5 consists of approximately 146,000 nodes, 89,000 hexahedron elements, 22,000 tetrahedron elements, 71,000 shell elements, 4,000 beam elements and a couple of discrete elements. The model uses 45 different material definitions in 380 parts. Figure 1 depicts the model release 1.5.

The model is delivered with a pre-stressed neck. Therefore, the bumpers in the neck use the feature `*Initial_Foam_Reference_Geometry`. The pre-tensioned cable/springs use offsets in the force displacement relation. The torsional beams are modeled by `*Constrained_Joint_Stiffness_Generalized` with local coordinate systems attached to the washers. These features allow that a once positioned dummy can be used as an ASCII input file without losing any pre-stress in the model in the neck and the spine. Consequently, the common procedure to use the `*Include` command to generate a final input is still applicable. The determination of pre-stress is presented in [3].

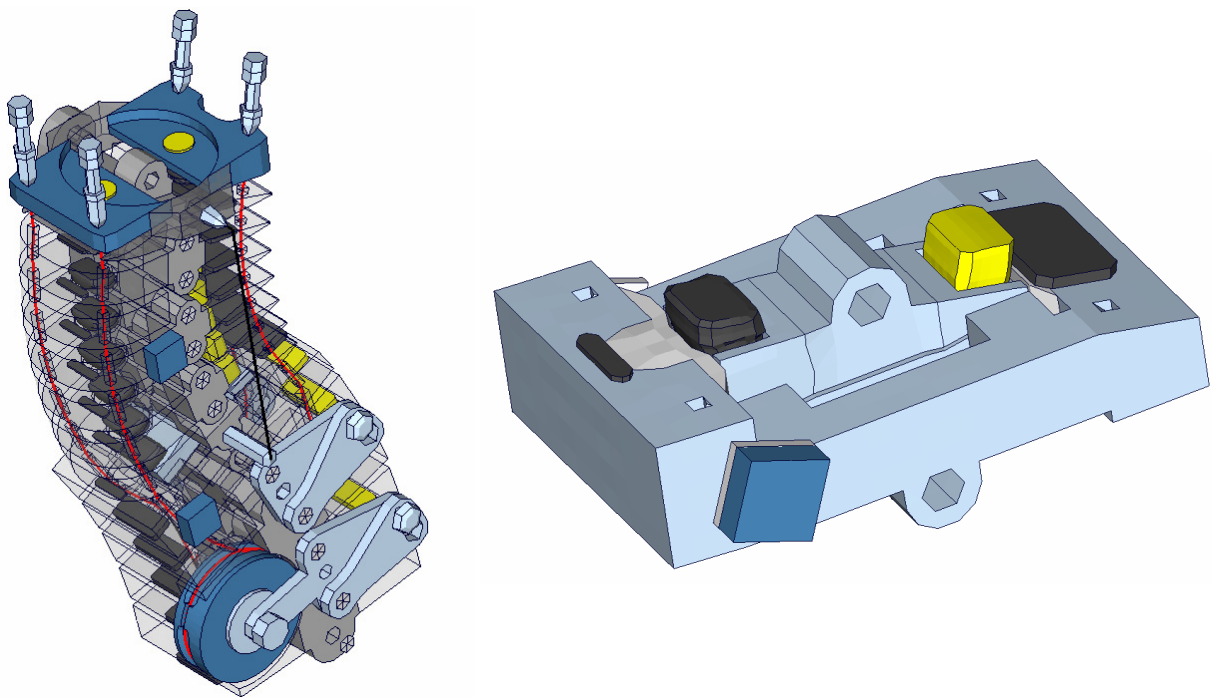


Figure 2: Selected parts of dummy model. Left: Neck model, with steel cable in red. Right: new modeled T1 load cell.

Most of the latest validation work is on the kinematics of the neck. Thereby the T1 load cell (see Figure 2 right hand side) is refined and modeled more accurate. The rubber bumpers are now modeled in a pit which hinders the lateral strain. The black vertebra stopper in Figure 2 right behind the yellow bumper is oriented to the measured position from the hardware dummy. Also the silicon charge of the gaps in the load cell is modeled at selected points.

Also the rotation relationship between the vertebrae will be added in next release. Due to the geometry of the neck vertebrae C2 – C7 the relative rotation between these vertebrae is hindered for rotations to the front. The rotations to the back are not hindered. This relationship is modeled also in use of the keyword `*CONSTRAINED_JOINT_STIFFNESS_GENERALIZED`. There we use an angle dependent friction moment to capture the hindered rotation of the vertebrae to the front.

Furthermore the development was on the material of the rubber bumpers. The latest official release uses the `*MAT_MOONEY-RIVLIN_RUBBER` for these parts. The next release will use the `*MAT_SIMPLIFIED_RUBBER` for the bumpers to enhance the kinematics and the strain rate

dependency of the rubber bumpers. Therefore the keyword `*INITIAL_FOAM_REFERENCE_GEOMETRY` had to be added in LS-DYNA for this material model. That is the reason why the next release of the BioRID-II must be used under LS-DYNA 971.

This step in the development of the BioRID-II was necessary because of the very sensitive kinematics of the neck. In use of the `*MAT_SIMPLIFIED_RUBBER` we are able to capture much more details for the neck kinematics and the oscillation problem of the upcoming releases is decreased in validation test a lot.

The BioRID-II model can be handled like the common Dummy FE-Models. The extremities can be positioned in use of a normal pre-processor. To pre-stress the BioRID-II model there are no other files necessary. The pre-stress is applied full automatically by LS-DYNA, also after a positioning simulation where the spine is deformed. Thereby the familiar functioning with dummies remains constant.

3 Material tests, component tests and fully assembled dummy test

A significant effort was made to generate a database on the static and dynamic material behavior, and the dummy behavior in component and fully assembled tests. A more detailed description of the material tests is presented in [4].

3.1 Material tests

For each important material in the BioRID-II different tests with static and dynamic tension and compression loads were performed. The considered strain rates vary from 0.001 to 500 1/s. Figure 3 shows some selected material samples which are used for the material tests. The tests were chosen to obtain material data that could be used with very small adaptations for material `*MAT_FU_CHANG_FOAM` and `*MAT_SIMPLIFIED_RUBBER`.

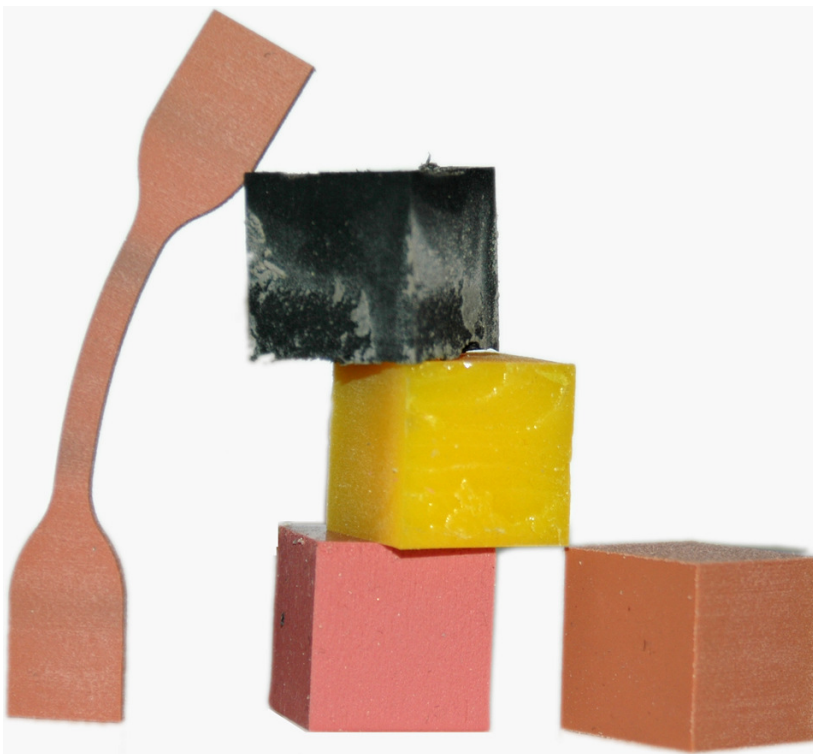


Figure 3: Material blocks for compression tests and a tension test sample.

3.2 Component tests

To get more understanding on the kinematics of the spine component tests were performed. Most of these tests are done only with the spine and the assembled head. In Figure 4 and Figure 5 different component tests are depicted. The tests were performed with different pulses, with fully and with partially equipped spine

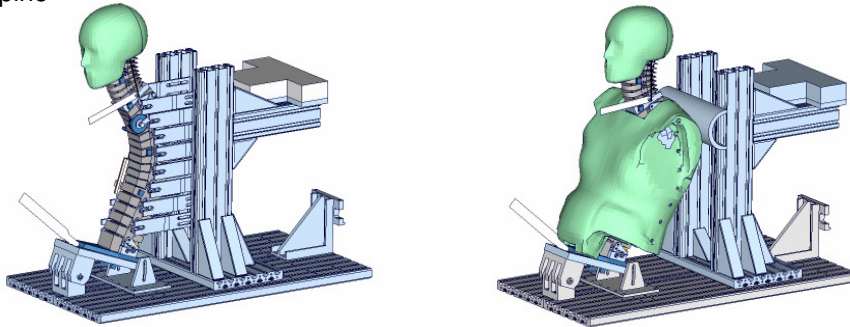


Figure 4: Left: BioRID II component test with supported spine. Right: Component test of assembled thorax.

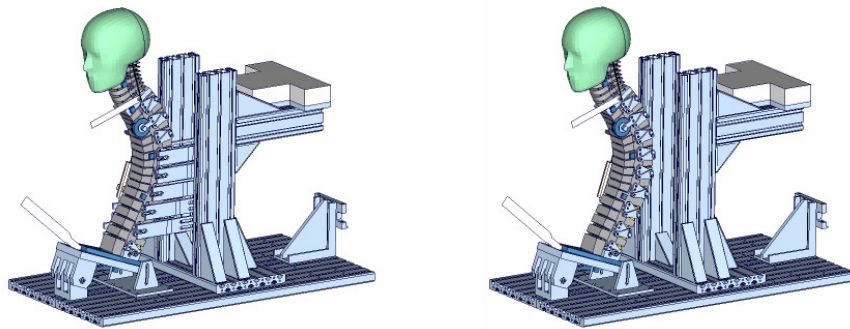


Figure 5: Left: BioRID-II component test with partially supported spine. Right: Component test with not supported spine.

More details are presented in [4]. The performance of the current release in the extensive number of tests is presented in the user manual of the dummy model [2].

Exemplarily, a test with spine fixed to the sled from the spine adapter plate up to the T1 vertebra is showcased in the following. Hence, only the neck with the assembled head can move. This load case is depicted in Figure 4 on the left hand side. The neck is equipped with damper and the pre-stressed steal cable. Figure 6 depicts the model at different stages during the test.

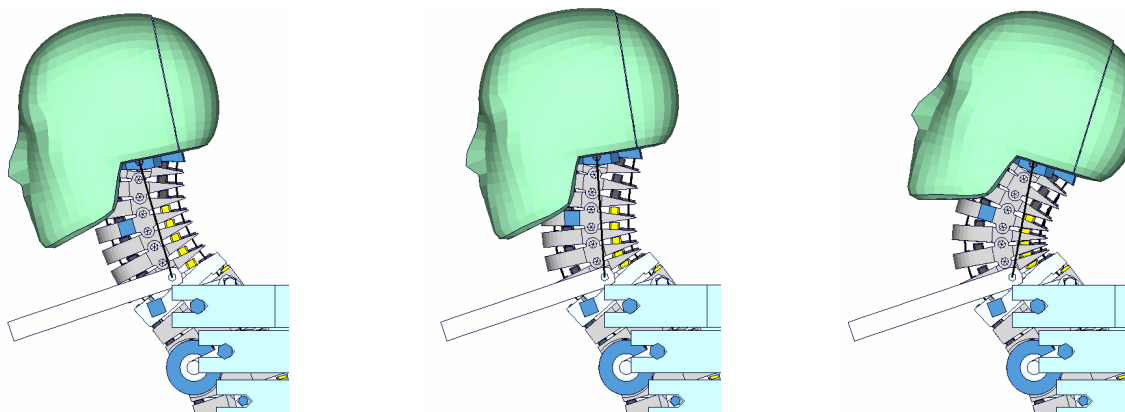


Figure 6: Spine, neck, and head during component test at 0, 45, and 125 ms.

It is broad to see that in the first 45 ms the head is only rotating a little bit. Most of the movement is a translation to the back and thereby the deformation looks like a shear deformation between the head and the T1 vertebra. This motion in the first few milliseconds is very dependent on the pre-stress, the

lateral strain of the rubber bumpers and the right rotation relationship between the vertebrae. Figure 7 to Figure 11 show the results of this load case.

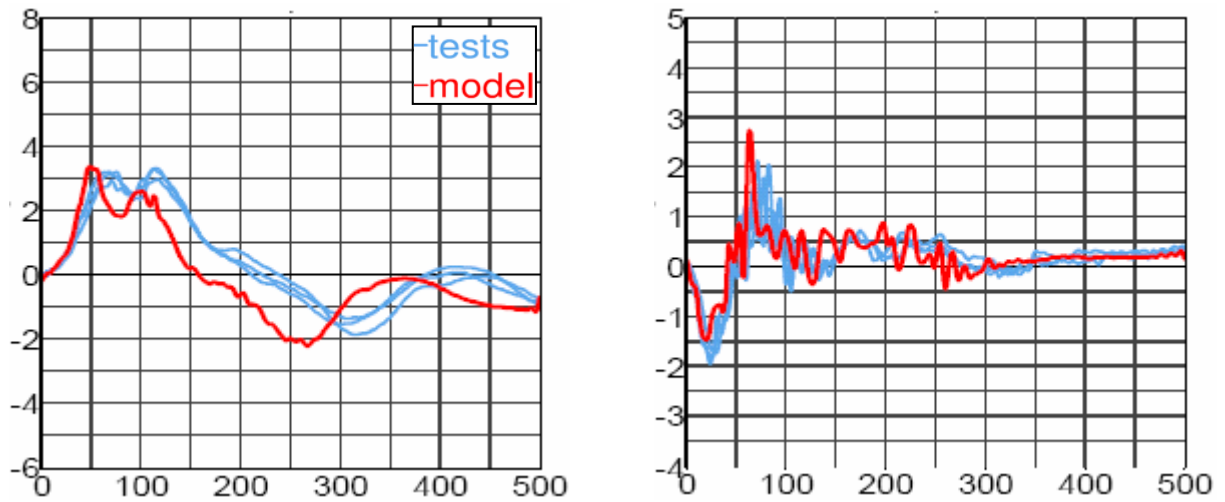


Figure 7: Head acceleration [g] vs. time [ms]. Left: x-acceleration. Right: z-acceleration.

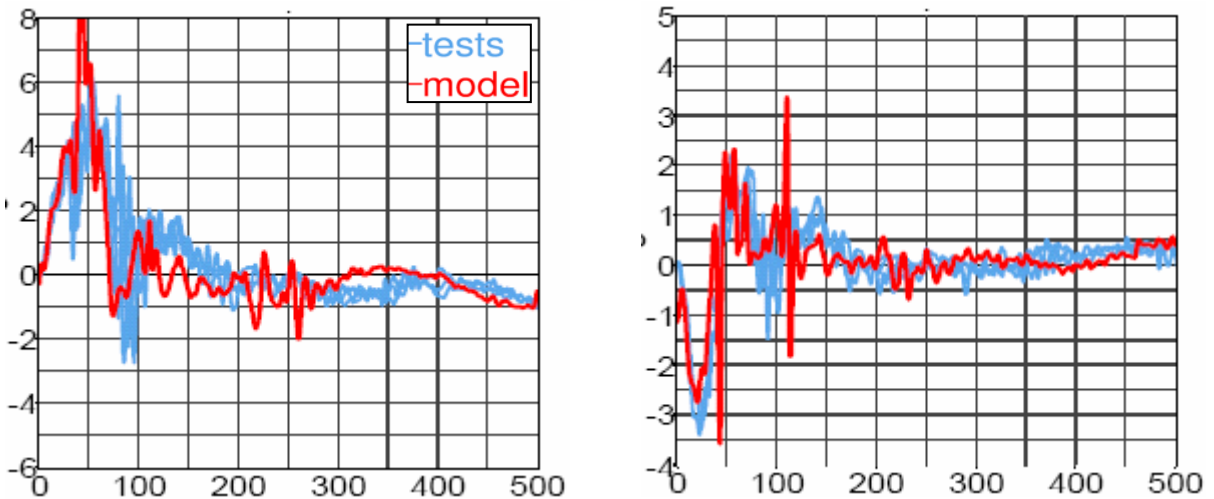


Figure 8: Neck acceleration [g] vs. time [ms] at C4. Left: x-acceleration. Right: z-acceleration.

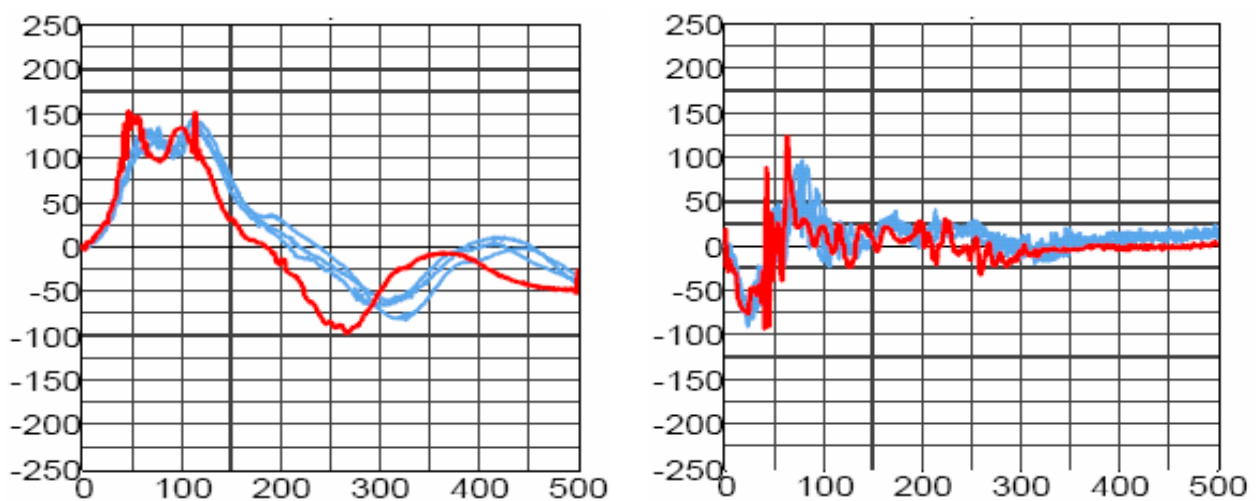


Figure 9: Upper neck force [N] vs. time [ms]. Left: Force in x. Right: Force in z.

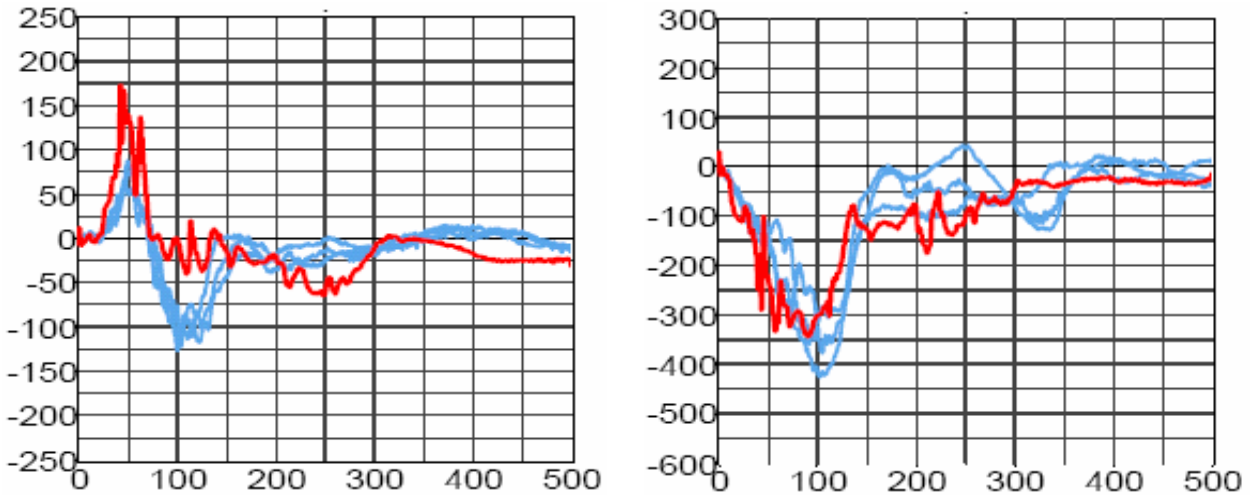


Figure 10: Lower neck force [N] vs. time [ms]. Left: Force in x. Right: Force in z.

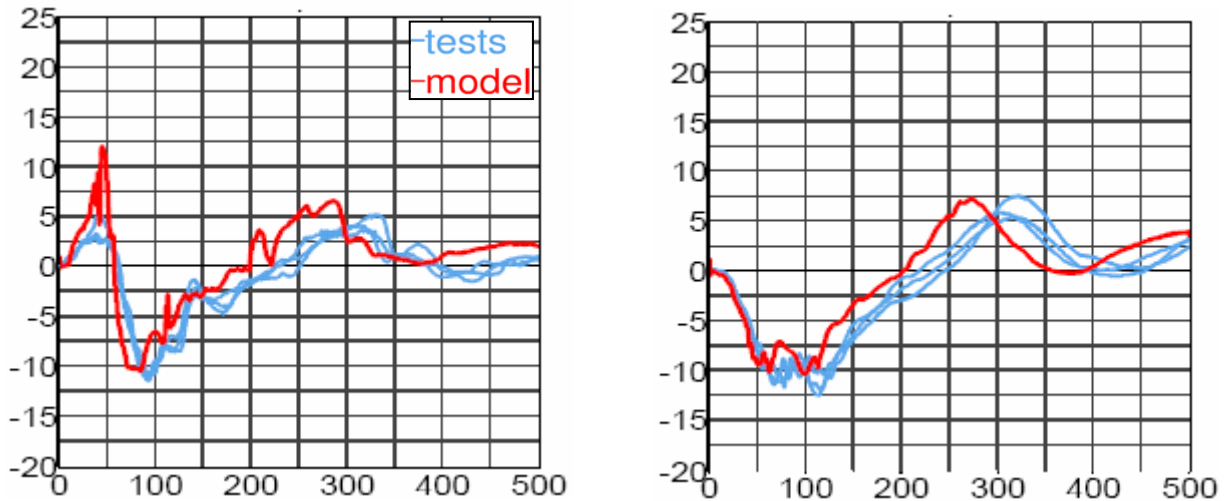


Figure 11: Left: Upper neck moment [Nm] along y vs. time [ms]. Right: Lower neck moment [Nm] along y vs. time [ms].

The double peak in the head x-acceleration (Figure 7 left) and in the upper neck x-force (Figure 9 left) is determined by the frictional dependency between the vertebrae. Also the peak in Figure 11 on the left hand side for the upper neck y-moment has a high dependency of these friction values. It looks like that the results of the shown model are a little bit too stiff.

Also the oscillation problem of T1 is decreased very much by using the new material model for the rubber bumpers. An example therefore is depicted in Figure 12.

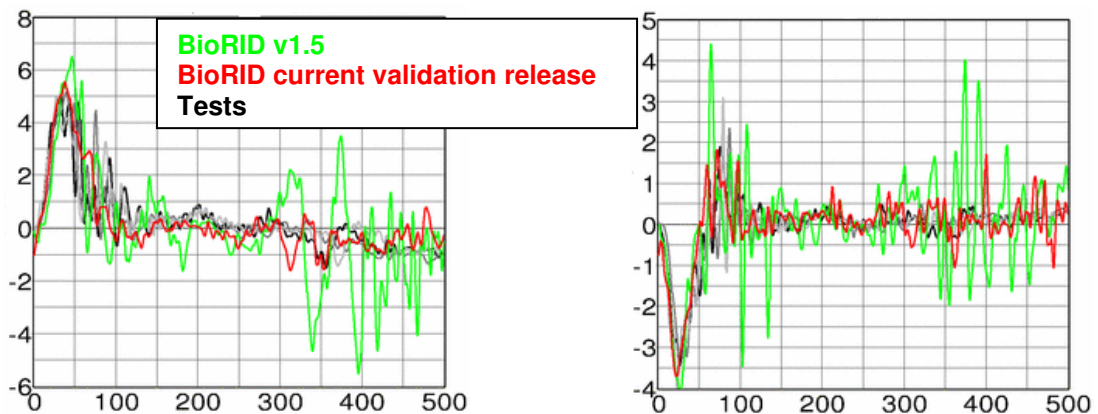


Figure 12: Neck acceleration [g] vs. time [ms] at T1. Left: x-acceleration. Right: z-acceleration.

This is a comparison between BioRID v1.5 (green line) and the current validation release (red line). The black lines are the test results. The shown test is depicted in Figure 5 on the left hand side. The spine is fixed to the sled from the pelvis adapter plate up to T8. The thoracic and neck vertebrae can move freely. The oscillations in the current validation release are much less than in the release v1.5 of the BioRID.

3.3 Full assembled dummy tests

Since the current seat systems are very complex a simplified seat system was used to validate the dummy model. The seat used for the tests, is a modified version of a seat that originally was built at Chalmers University to develop the BioRID dummy [5]. This simplified seat is depicted in Figure 13.

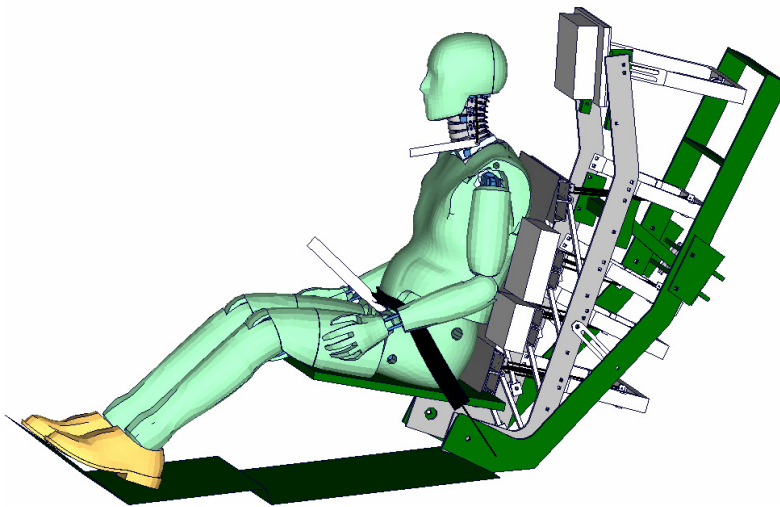


Figure 13: Full assembled dummy test.

The seat is loaded with three different pulses. The pulses are used from the EuroNCAP proposal for whiplash tests. In the following Figures the results of a 5g trapezoidal pulse are shown. For detailed information about the functionality of this seat please use the document [4]. The BioRID release on the seat is the same as in the component test in chapter 3.2. The results of the simulation are the red lines and the test results are the blue lines.

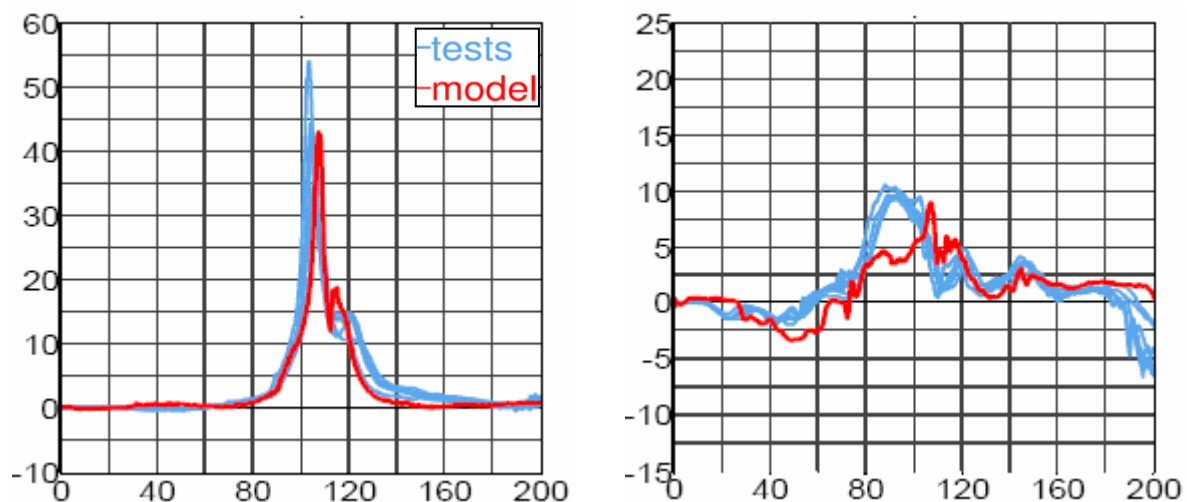


Figure 14: Head acceleration [g] vs. time [ms]. Left: x-acceleration. Right: z-acceleration

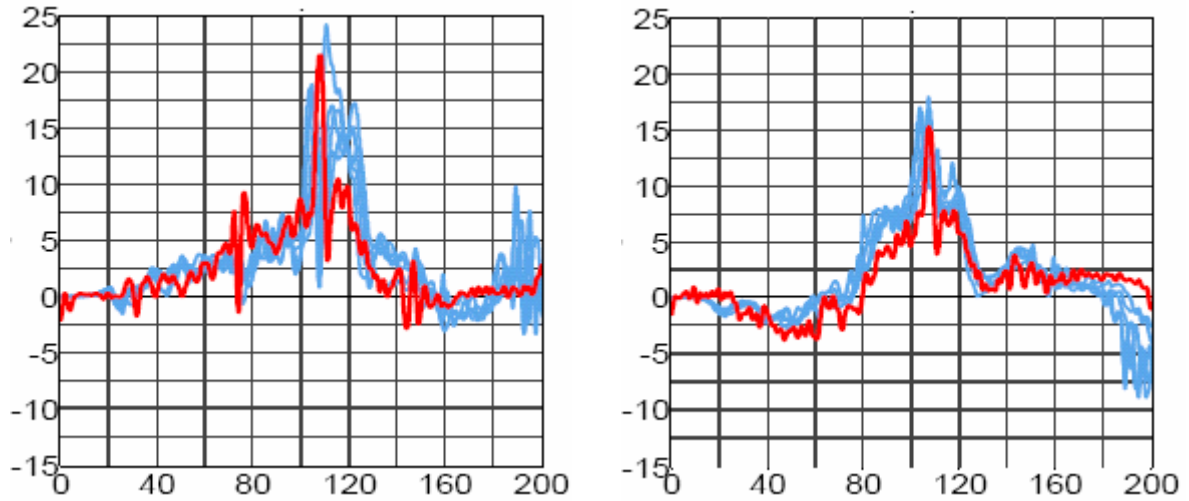


Figure 15: Neck acceleration [g] vs. time [ms] at C4. Left: x-acceleration. Right: z-acceleration.

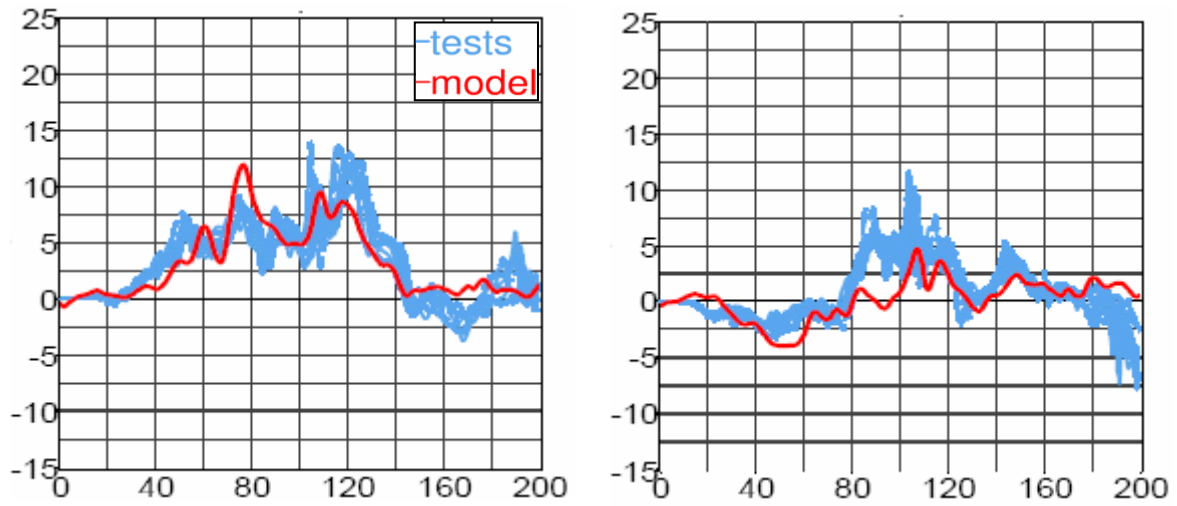


Figure 16: Upper spine acceleration [g] vs. time [ms] at T1. Left: x-acceleration. Right: z-acceleration.

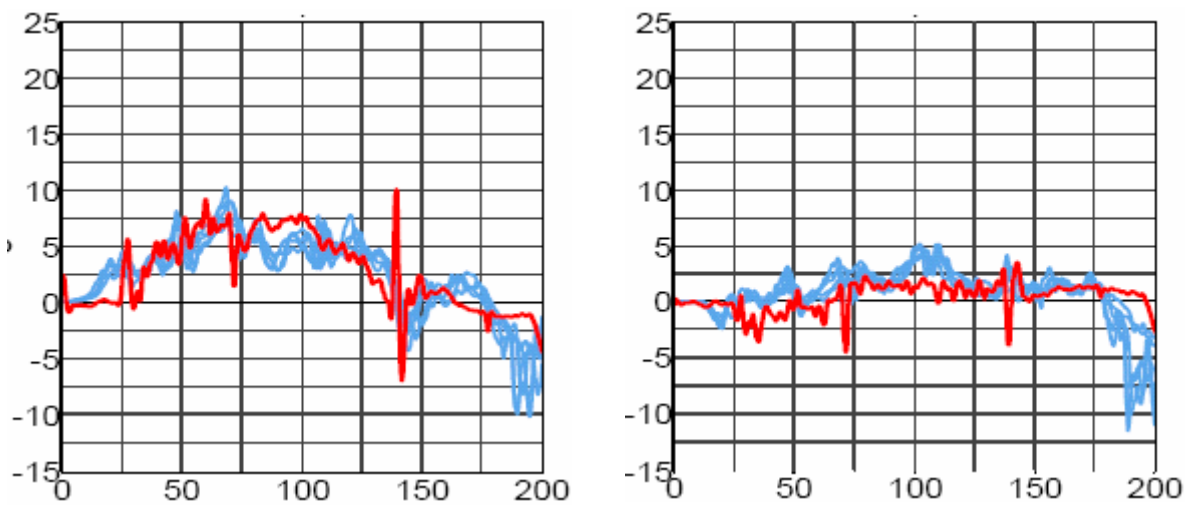


Figure 17: Spine acceleration [g] vs. time [ms] at T8. Left: x-acceleration. Right: z-acceleration.

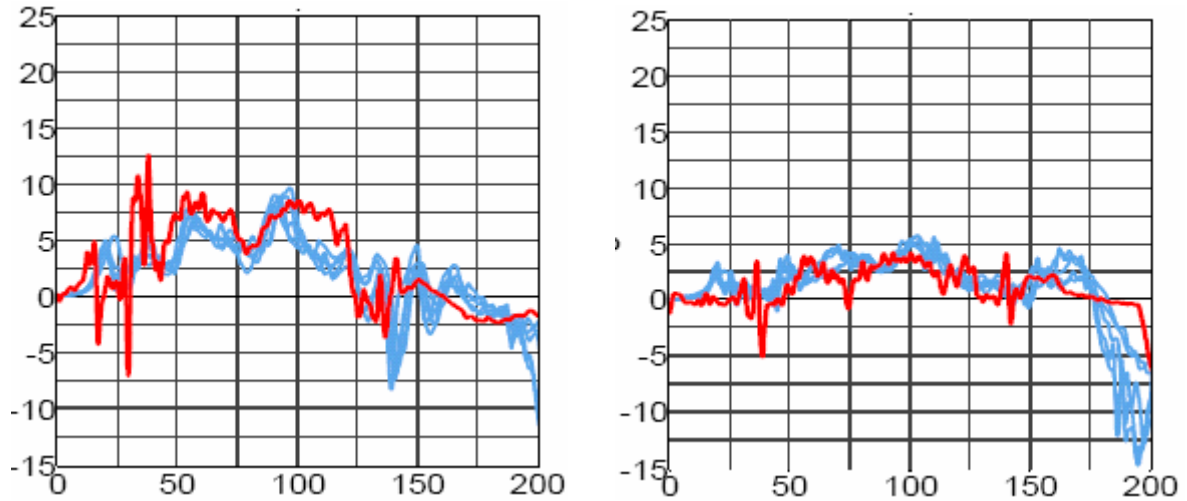


Figure 18: Spine acceleration [g] vs. time [ms] at L1. Left: x-acceleration. Right: z-acceleration

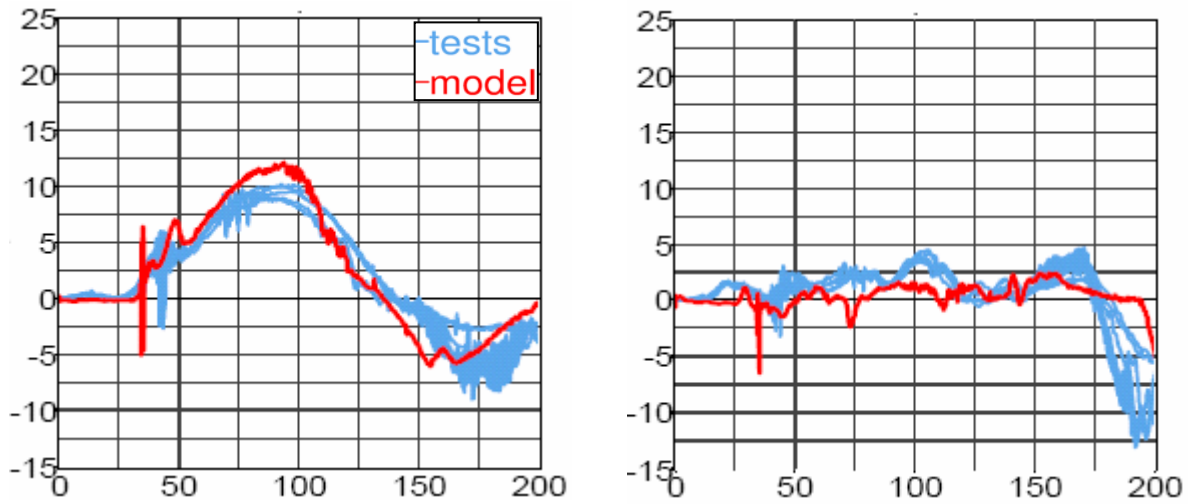


Figure 19: Pelvis acceleration [g] vs. time [ms]. Left: x-acceleration. Right: z-acceleration

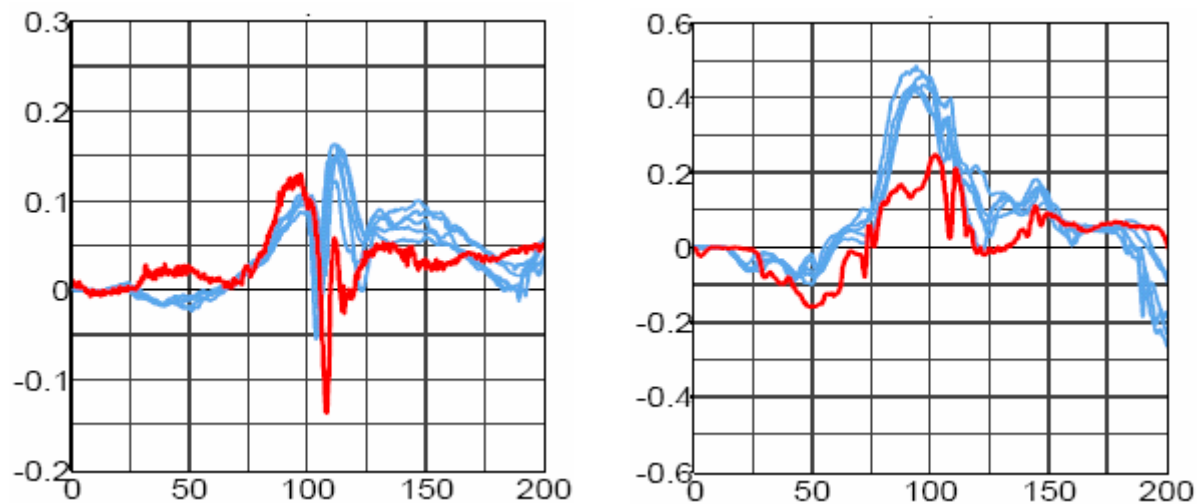


Figure 20: Upper neck force [kN] vs. time [ms]. Left: Force in x. Right: Force in z.

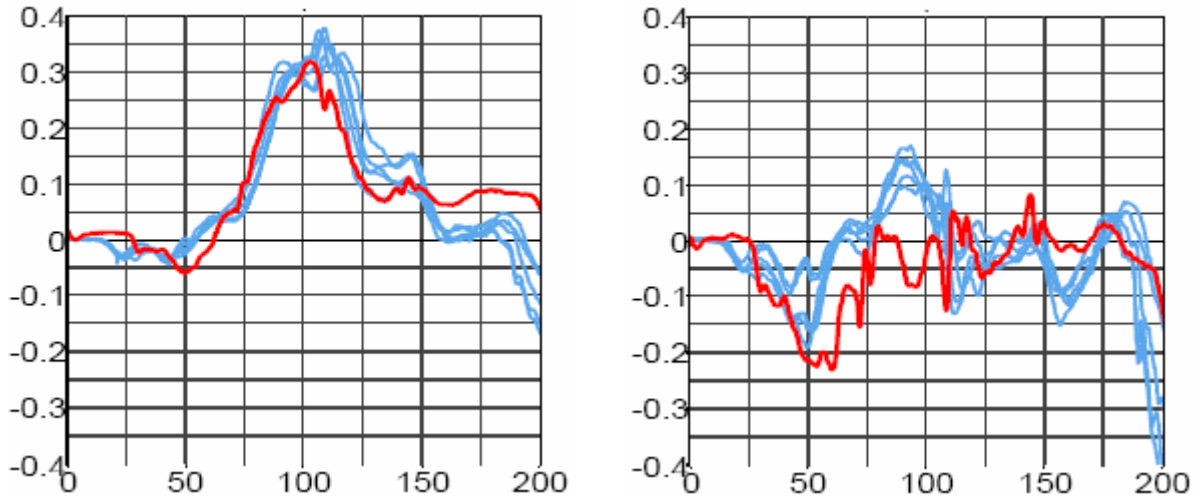


Figure 21: Lower neck force [kN] vs. time [ms]. Left: Force in x. Right: Force in z.

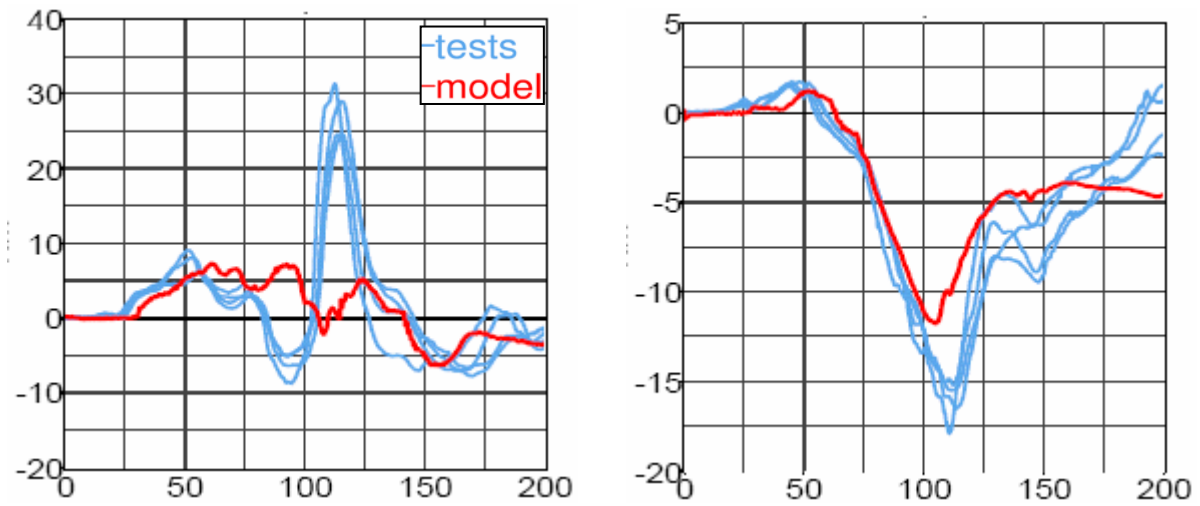


Figure 22: Left: Upper neck moment [Nm] along y axis vs. time [ms]. Right: Lower neck moment [Nm] along y axis vs. time [ms].

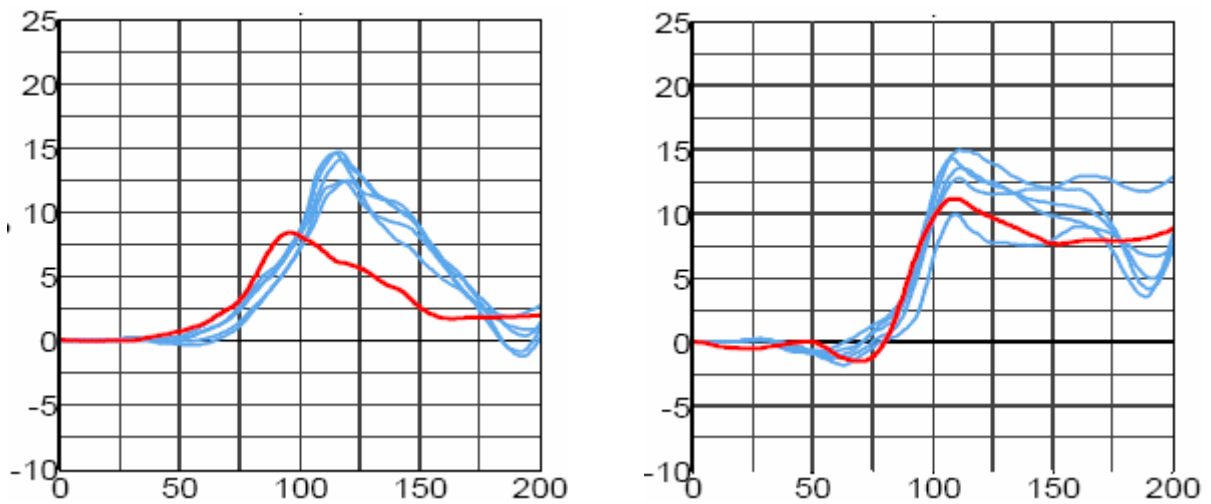


Figure 23: Left: OC neck link rotation [degree] vs. time [ms]. Right: T1 neck link rotation [degree] vs. time [ms].

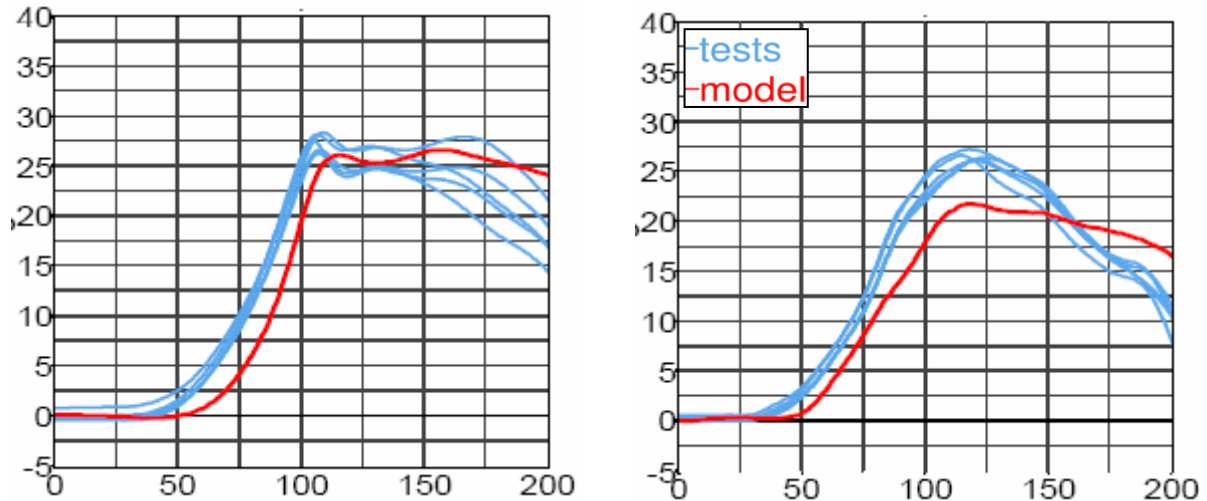


Figure 24: Left: global rotation of head [degree] vs. time [ms]. Right: global rotation of T1 [degree] vs. time [ms].

The results of this load case represent the performance of the model quite good for all other validation results. The accelerations are captured very well. The forces and moments are in a good range, but there is more capability for increasing the performance of the BioRID-II. The perversions of the neck link, head and T1 are very difficult to capture. These signals are much more sensitive than the forces and moments. But they also help us to understand some wrong signals like the upper neck moment in Figure 22 on the left hand side.

The reason for the wrong curve characteristic can be seen in the Figure 23 on the left hand side. The neck link rotation is too small and thereby the moment arms are different on the upper neck load cell. The too small angle results the different characteristic of the moment.

For the next official release we try to capture all these details. The oscillation problem of T1 is decreased very much by using the new material model for the rubber bumpers.

The model is easy to handle, even with the pre-stress. Most of the further work is now on the uncertainties of the model like friction values in the dummy and between dummy and seat. Therefore we spend a lot of time in a robustness analyze of the load case in this chapter 3.3.

4 Stochastic Investigations

In the following we focus on the question which parts have major influences on which. Initially we received this information by sets of single simulations by varying parameters in the input file. Obviously, investigations by running single simulations are limited. Since with LS-OPT provides a comfortable tool to investigate the model with stochastic methods LS-OPT was applied to perform a robustness analysis. In the following selected conclusions of the stochastic analysis are presented.

We used the full assembled dummy test of chapter 3.3 also with a 5g trapezoidal pulse for the stochastic investigations. Some material data, load curves, friction coefficients or damping constants used in the simulation are obtained from tests, so the values may have some variations. The defined variables are described in Table 1. Unfortunately, the performed tests do not allow determining the variation of the materials. Hence, the scatter of the different parameters was derived from simple physical assumptions. The distributions of puls 1 and puls 2 are based on test results. A normal distribution is always used if a target value is known; this target value is the mean value of the distribution.

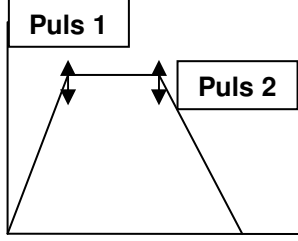
variable	description	Distribution		
			lower	upper
mat1010	Material of rubber bumpers yellow. Scale factor of ordinate values for all strain rates.	uniform	0.0004	0.0012
mat1011	Material of rubber bumpers black. Scale factor of ordinate values for all strain rates.	uniform	0.0004	0.0012
mat1025	Material of silicon torso flesh. Scale factor of ordinate values for all strain rates for material.	uniform	0.0006	0.0014
elbow	Rotational stiffness of elbows. Frictional moment limiting value for rotation of elbows.	uniform	3.5	7.0
should	Rotational stiffness of shoulder yokes. Frictional moment limiting value for rotation of shoulder	uniform	12	24
mat1119	Material of pelvis foam. Scale factor of ordinate values for all strain rates.	uniform	0.0007	0.0013
damper	Rotational damper. Damping moment per pitch rate.	uniform	0.2	1.0
con5502	Contact seat to dummy static and dynamic coefficient of friction	uniform	0.05	0.4
con5514	Contact black rubber mat of seat to back of dummy static and dynamic coefficient of friction	uniform	0.2	0.9
con5501	Contact of breaking system in the seat static and dynamic coefficient of friction for	uniform	0.01	0.3
mat5506	steal plate of the seat breaking system in the seat scale factor for ordinate values for all strain rates (back frame stiffness)	uniform	0.6	1.0
fric	Steal cable friction in the BioRID neck. Coulomb dynamic friction coefficient.	uniform	0.05	1.3
Puls 1	Acceleration pulse of sled. The variation of the trapezoid pulse is done by the variation of the vertex of the pulse. This variation is observed in the physical tests. 	normal	mean 5.0	std 0.25
Puls 2		normal	mean 5.0	std 0.05

Table 1: variables used in stochastic analysis

The responses considered in the analysis are listed in Table 2.

response	Description
max_Head_y_angle	maximum angle of head rotation
max_T1_y_angle	maximum angle of T1 rotation
Max_Pelvis_x_accel	maximum pelvis x acceleration
min_lower_Neck_y_moment	minimum peek value of lower neck y moment
max_lower_Neck_x_force	maximum peek value of lower neck x force
NIC	Neck Injury Criteria

Table 2: responses evaluated for the stochastic investigation

Most figures in this section were created using the software D-SPEX. It is software to explore the design space and to evaluate relationships between variables and responses. Currently, D-SPEX is a stand-alone product from DYNAMore initiated by Audi AG [6], but it will be implemented in LS-OPT. D-SPEX allows the visualization of 2-dimensional curve plots as well as 3-dimensional surface plots. For an n-dimensional problem, where n is the number of design variables and $n > 2$, one or two variables can be selected while the other variables values can be varied by a slider. In addition, it is possible to visualize statistical values like mean values and standard deviations, the correlation matrix or ANOVA results.

4.1 Monte Carlo Analysis

The idea of a Monte Carlo Analysis is to evaluate the responses at randomly generated sampling points. From the results of these simulations, mean values, standard deviations and other stochastic values can be computed. Here, a Latin Hypercube sampling has been used to generate 200 sampling points. The standard deviation is a measure for the scatter of a random variable around its mean value. The smaller the standard deviation the more the values accumulate around the mean value.

Example: Normal Distribution (Gauss)

The mean value is denoted by μ and the standard deviation by σ .

If a random variable has a normal distribution, the probability that the value is between $\mu - \sigma$ and $\mu + \sigma$ is 0.68 = 68% what is the marked area in Figure 25. The probability that the value is between $\mu - 2\sigma$ and $\mu + 2\sigma$ is 0.955 = 95.5%.

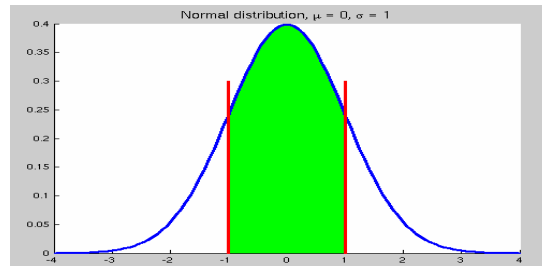


Figure 25: y Density function of probability for normal distribution.

For the Monte Carlo Analysis of BioRID-II, 14 variables and 6 responses are selected, so every simulation point has 20 dimensions. In the following the correlation of one result over a selected variable is depicted.

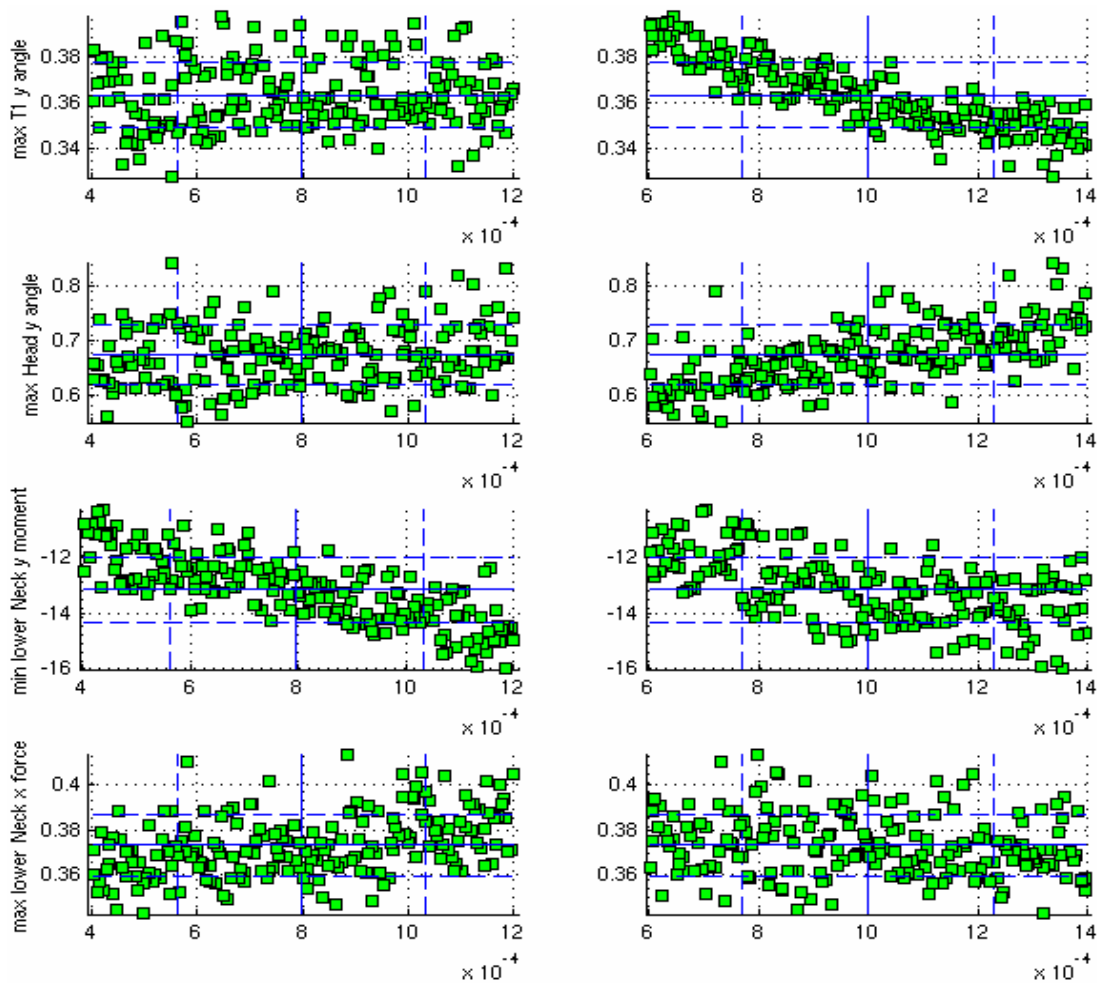


Figure 26: Anthill plot: max_Head_y_angle, max_T1_y_angle, min_lower_Neck_y_moment and max_lower_Neck_x_force over mat1010 and mat1025 respectively.

In Figure 26 the Anthill plots of the response values for maximum Head y angle, maximum T1 y angle, maximum lower neck x-force and the minimum of lower neck y-moment about the appropriate values of the variables material of the yellow rubber bumpers (mat1010) and the material of the torso flesh (mat1025). The solid lines mark the mean values, the dashed lines mark the standard deviations.

One conclusion is that the values of the responses depend on the values of mat1025. The torso flesh material has a distinctive influence on the T1 and Head rotation. If the stiffness of the material is increased, the maximum rotation of T1 is decreasing and the maximum rotation of the Head is increased. The dependency of the torso flesh to the T1 and Head rotations is clearly to see. The stiffness of the torso flesh is varied by about $\pm 40\%$ but the change of the T1 rotation is about $\pm 10\%$.

The influence of all other variables is much lower. It is not possible to draw any conclusions on the significance of the variable mat1010, because the variation of the responses may be caused by other variables.

Figure 27 shows the coefficients of correlation for all responses. If the absolute value of the correlation coefficient is close to one, the field is marked red, if the value is close to zero, the field is marked green. Again, the result that the variation of variable mat1025 has the highest influence on the values of the responses Head and T1 rotation. Also the variable puls 1 has an influence of the T1 and Head rotations but its lower then the influence of the torso flesh (mat1025). That means that the scatter of the T1 and Head rotation in Figure 24 could come from the variation of the pulse in the physical tests.

A further interesting dependence is the peak value of lower neck y moment. It depends much more on the stiffness of the yellow rubber bumpers (mat1010) than on the black rubber bumpers (mat1011).



Figure 27: correlation matrix

Because of the highest influence of the torso flesh material on the responses in the following there are plotted some selected history plots which show the results of all simulations. The different colors show the value of the variable mat1025 (torso flesh stiffness) in the single simulation but the history plots show the distribution generated by all variables.

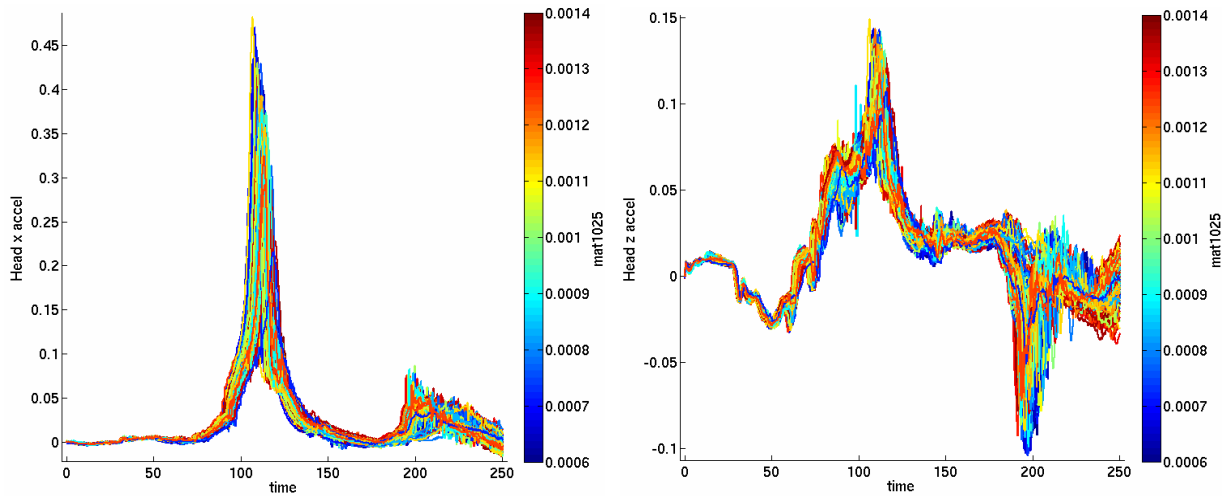


Figure 28: Head acceleration $[mm/ms^2]$ vs. time $[ms]$. Left: x-acceleration. Right: z-acceleration.

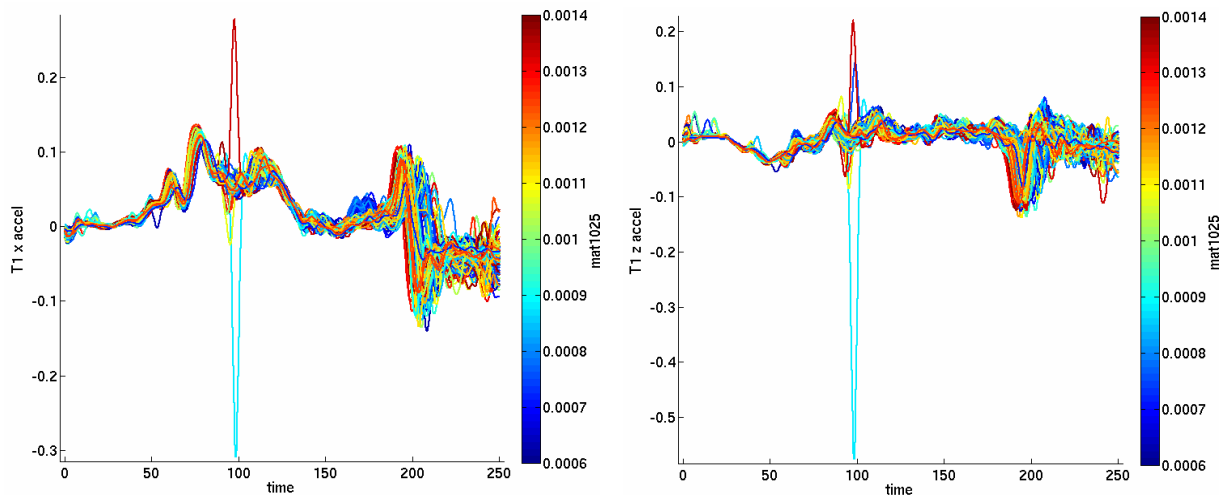


Figure 29: T1 acceleration $[mm/ms^2]$ vs. time $[ms]$. Left: x-acceleration. Right: z-acceleration.

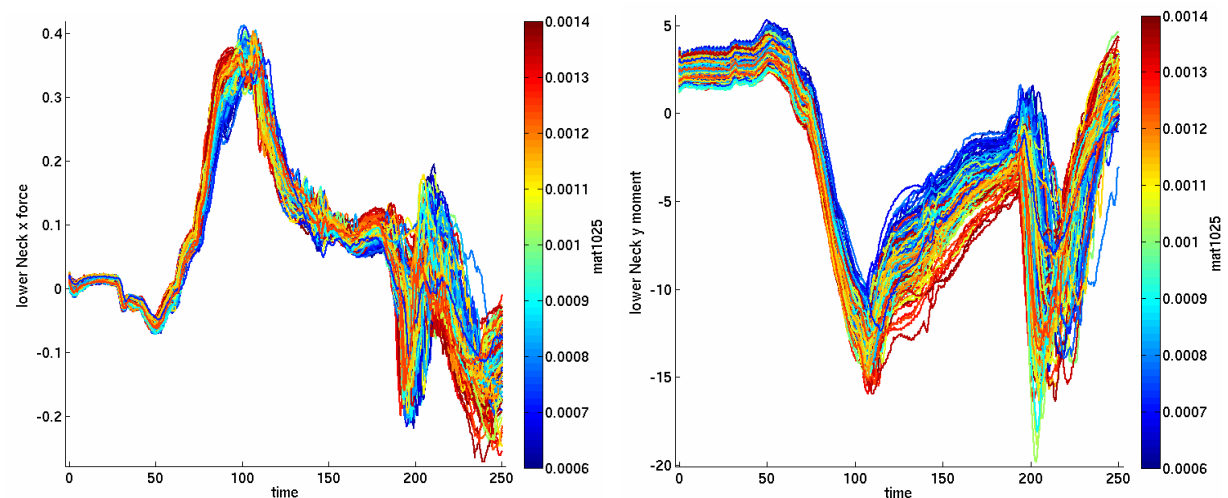


Figure 30: Left: lower Neck x force $[kN]$ vs. time $[ms]$. Right lower Neck y moment $[kNmm]$ vs. time $[ms]$.

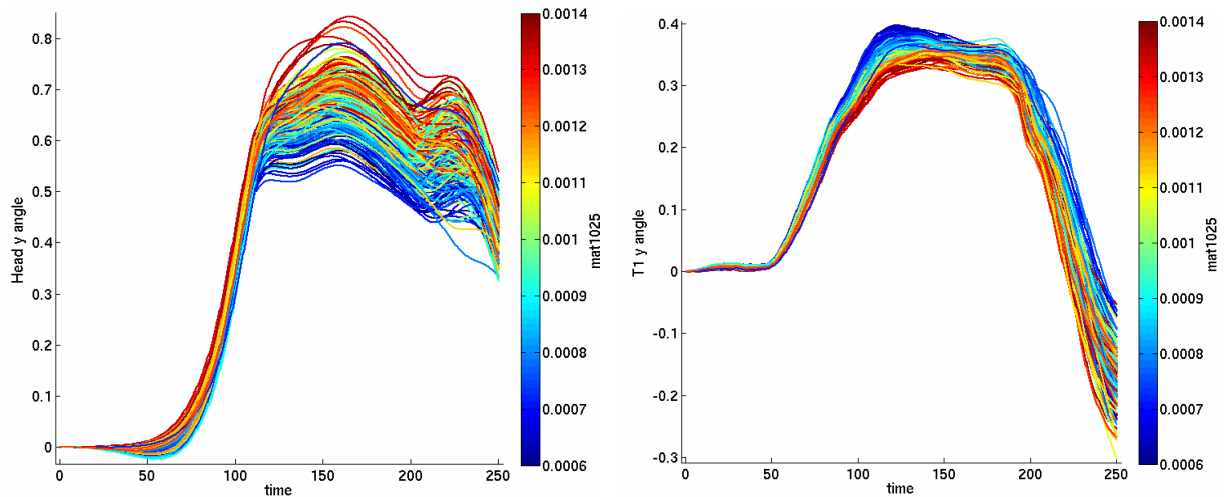


Figure 31: Left: Head global rotation [radian] vs. time [ms]. Right: T1 global rotation [radian] vs. time [ms].

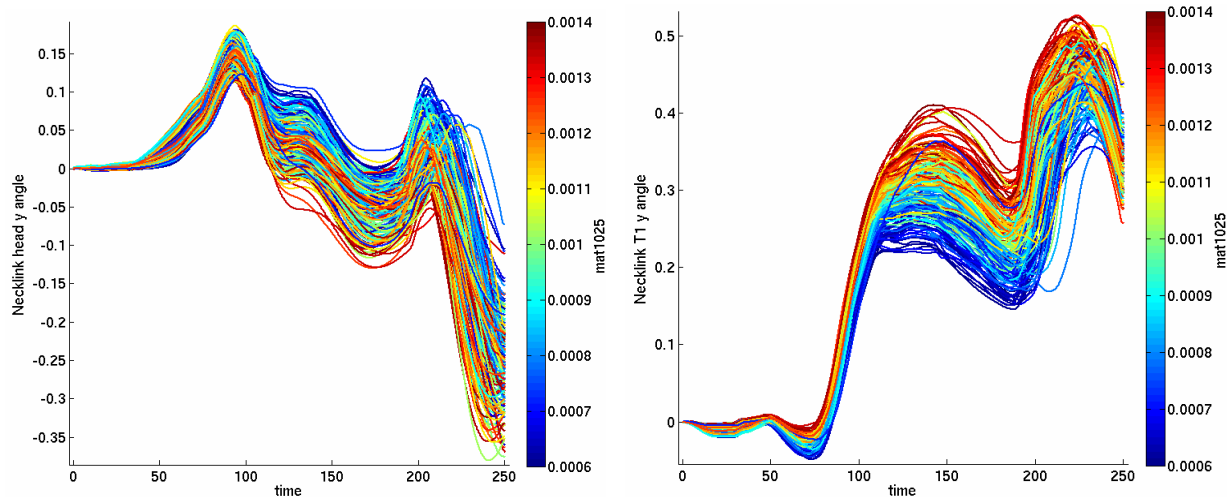


Figure 32: Left: Neck link rotation head vs. time [ms]. Right: neck link rotation T1 angle [radian] vs. time [ms].

If there is a tendency visible in the colour, the variable is significant for the response, else there can't be drawn any conclusion, because the variation may be caused by a variable that is not considered, compare to the Anthill plots.

In the time history plots it is easy to see, that the accelerations scatter less than the forces, moments and rotations. This is the reason why the accelerations are mostly easier to predict than some other signals like forces and moments. This observation was also made in [4].

A further interesting observation we can see is in Figure 29. In some special situations the acceleration of T1 shows very high peak values. These values are very difficult to handle if we try to extract injury criteria link the NIC from this signals. This peek values destroy the scalar values of the injury criteria.

Also notable is, that no observed signal in the history plots is changing its shape. The course of the curves is every time similar.

Using DYNastats in LS-OPT, statistical values may also be fringed on the FE model. DYNastats computes the values and they are displayed in LS-PrePost. In Figure 33 and Figure 34, the mean

value and the standard deviation of the x-displacement are fringed on the FE model. We observe the highest standard deviation at the hand of the dummy, because they are not fixed. At the head, the variation is also quite large because of the different rotations of the Head.

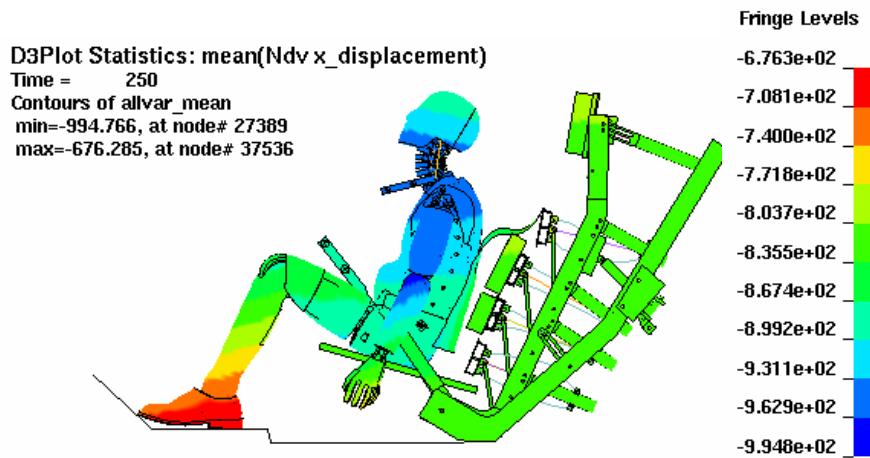


Figure 33: mean value for x-displacement fringed on FE model

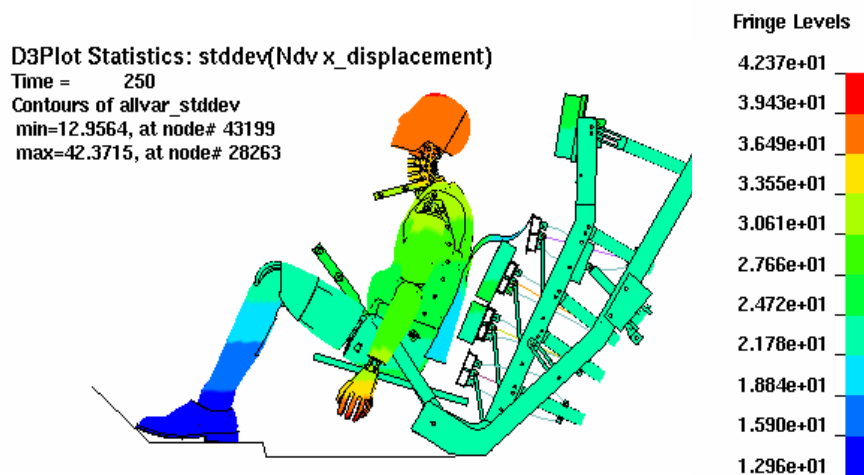


Figure 34: standard deviation for x-displacement fringed on FE model

The impression of the analyze is, that the accelerations are more robust than the forces, moments and rotations. Some new dependencies are found out in the model. Fore example the high influence of the yellow rubber bumpers on the lower neck moment.

In accordance to the physical test we see the same behavior as in the model. The accelerations scatter also less than the forces, moments and rotations (see Figure 14 - Figure 24).

5 Conclusions

The current release of the BioRID-II model for LS-DYNA is based on material, component and fully assembled dummy sled tests. By the use of the new material model of the rubber bumpers, the oscillations of the accelerations have decreased significantly. Because of the new material model for the rubber bumpers, the next release will require LS-DYNA 971. For selected platforms it is possible to supply an extended LS-DNA 970 version.

Important knowledge during validation was generated with optimization and robustness techniques. The paper presents a Monte Carlo analysis of one selected BioRID-II load case. The analysis shows that the scatter of the forces, moments and rotations are higher than of the accelerations. Hence, the dependencies and sensitivities are lower for predicted accelerations. This is in accordance with observations in [4] that signals like accelerations are easier to predict than others like forces and moments.

A limitation of the Monte Carlo analysis is, that it is not possible determine which variable causes a higher scatter than another variables. Therefore, a Meta-Model-based Monte Carlo Analysis also provided by LS-OPT will be used for further investigations. Furthermore, using Meta-Models allows visualizing the n-dimensional results by projecting it to a 3-dimensional surface. Doing this interactively helps understanding the model behavior significantly. The presented methods will be used frequently during development of finite element models from DYNAmore.

6 Reverences

- [1] Whiplash (2004), Aspen Opinion, Aspen Re, UK.
- [2] FAT LS-DNYA BioRID II User's Manual (2006), Version 1.5, DYNAmore GmbH, Stuttgart, Germany.
- [3] P. SCHUSTER, S. STAHLSCHMIDT, U. FRANZ A. RIESER, H. KASSEGGGER, „Entwicklung des Dummymodells BioRID 2“, 4th LS-DYNA Forum 2005, Bamberg, Germany.
- [4] Stahlschmidt S., “BioRID II Dummy Model Development – Influence of Parameters in Validation and consumer Tests”, 9th International LS-DYNA Users Conference Detroit USA, 2006
- [5] BioRID-IIc Rear Impact Crash Test Dummy, James R. Kelly, Robert A. Denton, Inc.
- [6] Thiele M., Optimization of an Adaptive Restraint System Using LS-OPT and Visual Exploration of the Design Space Using D-SPEX, 9th International LS-DYNA Users Conference Detroit USA, 2006